ISSN 1070-3284, Russian Journal of Coordination Chemistry, 2015, Vol. 41, No. 3, pp. 149–161. © Pleiades Publishing, Ltd., 2015.
Original Russian Text © P.S. Koroteev, N.N. Efimov, Zh.V. Dobrokhotova, A.B. Ilyukhin, A.V. Gavrikov, V.M. Novotortsev, 2015, published in Koordinatsionnaya Khimiya, 2015, Vol. 41, No. 3, pp. 131–143.

Binuclear and Polynuclear Cymantrenecarboxylate Complexes of Heavy Lanthanides

P. S. Koroteev*, N. N. Efimov, Zh. V. Dobrokhotova, A. B. Ilyukhin, A. V. Gavrikov, and V. M. Novotortsev

Kurnakov Institute of General and Inorganic Chemistry, Russian Academy of Sciences, Leninskii pr. 31, Moscow, 119991 Russia

**e-mail: pskoroteev@list.ru*

Received September 15, 2014

Abstract—New binuclear cymantrenecarboxylate complexes of rare-earth metals, $[Ln_2(\mu\text{-}O,\eta^2\text{-}O_2CCym)_2(\mu_2\text{-}O,O'\text{-}O_2CCym)_2(\eta^2\text{-}O_2CCym)_2(DMSO)_4]$ (Ln = Tb (**I**), Dy (**II**); Cym = $(\eta^5\text{-}C_5H_4)Mn(CO)_3$) and $[Ln_2(\mu_2\text{-}O,O'\text{-}O_2CCym)_4(\eta^2\text{–}NO_3)_2(DMSO)_4]$ (Ln = Tb (**III**), Dy (**IV**)), are synthesized and characterized by X-ray diffraction analysis. The carboxylate clusters containing the Mn^{2+} ion, which is formed due to the destruction of the cymantrenenecarboxylate anion, $[Tb_4(\mu_3\text{-}OH)_4(\mu_2\text{-}O,O'\text{-}O_2CCym)_6(H_2O)_3(THF)_4][MnCl_4] \cdot 4CH_2Cl_2 \cdot 6THF$ (**V**) with the cubane-like structure, and $[Er_2Mn(\mu_2\text{-}O_2CCym)_6(\eta^2\text{-}O_2CCym)_2((MeO)_3PO)_4] \cdot 2MePh$ (**VI**) with linear structure, are also obtained. The magnetism of complexes **I**, **II**, **V**, and **VI** is studied in a direct magnetic field. The magnetic properties of complexes **II** and **VI** are studied in direct and alternating magnetic fields. Complex **II** exhibits the properties of a single-molecule magnet. The thermal decomposition of complexes **I**–**IV** is studied by differential scanning calorimetry and thermogravimetric analysis. According to the X-ray diffraction analysis data, the final thermolysis products of complexes **III** and **IV** in air are multiferroics $LnMn_2O_5$.

DOI: 10.1134/S1070328415030069

INTRODUCTION

Numerous 3*d*–4*f* complexes are known, including those of carboxylates in which different metal ions are linked through the polydentate ligands [1–4], whereas heterometallic 3*d*–4*f* carboxylates containing a transition metal in the organometallic fragments are poorly studied. Similar complexes are of both theoretical and practical interest, since they can potentially combine the properties of the rare-earth metal ion and organometallic fragment and can serve as precursors for mixed-oxide phases that are functional materials. Mainly ferrocene derivatives remained studied for a long time [5]. We have earlier synthesized and studied 3*d*–4*f* carboxylates containing the cymantrene fragment ($(\eta^5\text{-}C_5H_5)Mn(CO)_3$) and lanthanide ions of the cerium group. These complexes are binuclear, which is typical of rare-earth metal carboxylates [6–10]. In the structures of the transition metal cymantrenecarboxylate complexes, the O_2CCym ligands (Cym is $(\eta^5\text{-}C_5H_4)Mn(CO)_3$) also behave similarly to other carboxylates [11–14]. However, in the case of lanthanides of the yttrium group, binuclear cymantrenecarboxylates were synthesized only when dimethyl sulfoxide (DMSO) was used as an additional ligand. At the same time, the products containing Mn^{2+} ions formed due to cymantrenyl fragment destruction in solution were isolated in other cases. The syntheses and properties of new both binuclear and polynuclear cymantrenecarboxylate complexes of heavy lanthanides containing Mn^{2+} are described in this work.

EXPERIMENTAL

Commercial reagents and solvents were used for the syntheses: hydrated lanthanide nitrates and chlorides $LnCl_3 \cdot 6H_2O$ and $Ln(NO_3)_3 \cdot 5H_2O$ (Alfa Aesar), cymantrene (Aldrich), and solvents (MeOH, DMSO, $n\text{-}C_6H_{14}$, C_6H_5Me, CH_2Cl_2, $(MeO)_3PO$) (Alfa Aesar). Cymantrenecarboxylic acid was synthesized according to a known procedure [15]. Prior to use methanol was distilled over magnesium, DMSO was distilled in vacuo, hexane and toluene were successively distilled over P_2O_5 and sodium, and tetrahydrofuran (THF) was distilled over lithium aluminohydride. Attenuated total internal reflectance IR spectra were recorded in the range from 600 to 4000 cm^{-1} on an ALPHA instrument (Bruker). Microanalyses were performed on an EA1108 85 CHNS analyzer (Carlo Erba).

Syntheses of $[Ln_2(\mu\text{-}O,\eta^2\text{-}O_2CCym)_2(\mu_2\text{-}O,O'\text{-}O_2CCym)_2(\eta^2\text{-}O_2CCym)_2(DMSO)_4]$ (Ln = Tb (I), Dy (II)) and $[Ln_2(\mu_2\text{-}O,O'\text{-}O_2CCym)_4(\eta^2\text{–}NO_3)_2(DMSO)_4]$ (Ln = Tb (III), Dy (IV)) were carried

out using a procedure similar to that described in [8]. The difference in the syntheses was as follows: in the case of compounds **I** and **II**, the starting substances were chlorides $LnCl_3 \cdot 6H_2O$, $CymCO_2H$, and KOH in a ratio of 1 : 3 : 3, whereas nitrates $Ln(NO_3)_3 \cdot 5H_2O$, $CymCO_2H$, and KOH in a ratio of 1 : 2 : 2 were used in the case of compounds **III** and **IV**. The yields were 65–70%.

For $C_{62}H_{48}O_{34}S_4Mn_6Tb_2$ (**I**)

anal. calcd., %:	C, 35.25;	H, 2.29;	S, 6.07.
Found, %:	C, 35.35;	H, 2.25;	S, 6.05.

IR for **I** (KBr), ν, cm^{-1}: 2923w, 2852 w, 2018 w, 1920 s, 1626 m, 1575 m, 1556 w, 1536 w, 1493 m, 1485 m, 1416 w, 1396 m, 1356 m, 1313 w, 1195 w, 1058 w, 1028 m, 1011 m, 959 w, 936 w, 904 w, 844 w, 798 m, 777 w, 667 s, 633 s.

For $C_{62}H_{48}O_{34}S_4Mn_6Dy_2$ (**II**)

anal. calcd., %:	C, 35.13;	H, 2.28;	S, 6.05.
Found, %:	C, 35.18;	H, 2.21;	S, 6.03.

IR for **II** (KBr), ν, cm^{-1}: 2925 w, 2853 w, 2014 s, 1918 s, 1627 m, 1577 m, 1556 w, 1536 w, 1492 m, 1416 w, 1397 m, 1335 m, 1313 w, 1194 w, 1058 w, 1028 m, 1011 m, 936 w, 926 w, 904 w, 869 w, 844 w, 805 m, 798 w, 777 w, 667 s, 632 s.

For $C_{44}H_{40}N_2O_{30}S_4Mn_4Tb_2$ (**III**)

anal. calcd., %:	C, 30.33;	H, 2.31;	N, 1.61;	S, 7.36.
Found, (%):	C, 30.35;	H, 2.25;	N, 1.57,	S, 7.37.

IR for **III** (KBr), ν, cm^{-1}: 2925 w, 2853 w, 2015 s, 1914 s, 1627 m, 1575 m, 1556 w, 1486 m, 1460 w, 1417 m, 1395 m, 1357 m, 1309 m, 1291 w, 1194 w, 1058 w, 1012 m, 995 m, 956 m, 936 m, 928 w, 901 w, 852 w, 843 w, 803 m, 777 m, 754 m, 740 m, 708 w, 666 s, 632 s.

For $C_{44}H_{40}N_2O_{30}S_4Mn_4Dy_2$ (**IV**)

anal. calcd., %:	C, 30.20;	H, 2.30;	N, 1.60;	S, 7.33.
Found, %:	C, 30.23;	H, 2.24;	N, 1.57;	S, 7.35.

IR for **IV** (KBr), ν, cm^{-1}: 2925 w, 2852 w, 2031 m, 2015 m, 1944 m, 1925 s, 1910 s, 1630 m, 1551 w, 1483 m, 1456 m, 1415 m, 1394 m, 1359 m, 1306 m, 1291 w, 1057 w, 1036 m, 1017 m, 994 m, 954 w, 926 w, 855 w, 837 w, 818 w, 804 w, 793 w, 778 w, 739 w, 665 m, 631 s.

Synthesis of $[Tb_4(\mu_3\text{-}OH)_4(\mu_2\text{-}O,O'\text{-}O_2CCym)_6(H_2O)_3(THF)_4][MnCl_4] \cdot 4CH_2Cl_2 \cdot 6THF$ (V). $CymCO_2H$ (248 mg, 1 mmol) and KOH (56 mg, 1 mmol) were dissolved in methanol (6 mL). The solution was stirred for 20 min at room temperature, and a solution of $TbCl_3 \cdot 6H_2O$ (125 mg, 0.33 mmol) in methanol (4 mL) was added. The mixture was stirred for 20 h in an argon atmosphere. The reaction mixture was evaporated to dryness in a vacuum of a water-jet pump. The dry residue was extracted with hot (~60°C) THF (5 mL). Dichloromethane (2 mL) and hexane (3 mL) were added with stirring to the obtained solution, and the solution was filtered in vacuo through a glass filter. The crystals of complex **V** were formed in the reaction mixture for 3 weeks at room temperature. The yield was 34 mg (11.78% based on Tb).

For $C_{98}H_{122}O_{47}Cl_{12}Mn_7Tb_4$ (**V**)

anal. calcd., %:	C, 33.65;	H, 3.52.
Found, %:	C, 33.72;	H, 3.58.

IR for **V**, ν, cm^{-1}: 3789–3716 w, 2033 s, 1936 s, 1864 w, 1580 m, 1573 m, 1553 m, 1536 w, 1513 w, 1484 m, 1451 w, 1442 w, 1393 m, 1365 m, 1334 w, 1199 w, 1166 w, 1111 w, 1094 w, 1057 w, 1031 w, 927 w, 852 w, 842 w, 806 w, 784 w, 720 w, 693 w, 666 s, 691 s.

Synthesis of $[Er_2Mn(\mu_2\text{-}O_2CCym)_6(\eta^2\text{-}O_2CCym)_2((MeO)_3PO)_4] \cdot 2MePh$ (VI). $CymCO_2H$ (248 mg, 1 mmol) and KOH (56 mg, 1 mmol) were dissolved in methanol (6 mL). The solution was stirred for 20 min at room temperature, and a solution of $Er(NO_3)_3 \cdot 5H_2O$ (148 mg, 0.33 mmol) in methanol (4 mL) was added with stirring. The mixture was stirred for 24 h under an argon atmosphere, and then the reaction mixture was evaporated to dryness in a vacuum of a water-jet pump. The dry residue was extracted with hot (~60°C) THF (4 mL). Toluene (2 mL), $(MeO)_3PO$ (1 mL), and hexane (2 mL) were added with stirring to the obtained solution. The resulting solution was filtered in vacuo through a glass filter. The crystals of complex **VI** began to precipitate from the reaction mixture in 2 weeks at room temperature. The remaining product crystallized upon the subsequent storage of the reaction mixture at –20°C for a month. The yield was 47 mg (9.64% based on Er).

For $C_{91}H_{76}O_{56}P_4Er_2Mn_9$ (**VI**)

anal. calcd., %:	C, 37.84;	H, 2.72.
Found, %:	C, 37.77;	H, 2.68.

IR for **VI**, ν, cm^{-1}: 2017 s, 1916 s, 1586 m, 1573 m, 1567 m, 1556 m, 1485 m, 1454 m, 1392 m, 1363 m, 1255 m, 1231 m, 1193 m, 1042 s, 929 w, 855 m, 819 w, 807 m, 797 m, 783 w, 767 w, 729 w, 694 w, 666 s, 630 s.

The thermal decomposition of complexes **I–IV** was studied by differential scanning calorimetry (DSC) and thermogravimetric analysis. Thermogravimetric measurements in a flow of artificial air (the amounts were as follows: Ar >99.998%, O_2 <0.0002%, N_2 <0.001%, water vapor <0.0003%, and CH_4 <0.0001%) (20 mL/min) were carried out on a TG 209 F1 NETZSCH instrument with a heating rate of 10°C/min. The composition of the gas phase was

studied on a QMS 403C Aëolos mass-spectrometric attachment under the thermogravimetric experimental conditions. DSC studies in a flow of dried artificial air and argon were carried out on a DSC 204 F1 NETZSCH calorimeter at a heating rate of 10°C/min. The temperature calibration of the thermobalance and calorimeter was carried out by the phase transition points of the standard substances (C_6H_{12}, Hg, KNO_3, In, Sn, Bi, and CsCl; purity 99.99%) according to the ISO/CD 11357-1 norm. Thermal analysis data were processed according to the ISO 11357-1, ISO 11357-2, ISO 11358, and ASTM E 1269-95 standards using the NETZSCH Proteus Thermal Analysis program package.

Magnetic measurements were carried out on an PPMS-9 magnetometer (Quantum Design) in a range of 2–300 K and a magnetic field of 5 kOe. The paramagnetic components of the magnetic susceptibility (χ) were determined taking into account the diamagnetic contribution calculated from Pascal's constant. The effective magnetic moment (μ_{eff}) was calculated by the formula $\mu_{eff} = [(3k/N\beta^2)\chi T]^{1/2} \approx (8\chi T)^{1/2}$, where N is Avogadro's number, k is the Boltzmann constant, and β is Bohr's magneton.

X-Ray diffraction analysis. The experimental data for complexes **I–VI** were collected on a Bruker SMART APEX2 diffractometer ($\lambda Mo K_\alpha$ radiation, graphite monochromator) [16]. An absorption correction was applied using the semiempirical method by equivalents (SADABS) [17]. The structures were determined by a combination of a direct method and Fourier syntheses. The site occupancies of the disordered fragments were obtained by the isotropic refinement of the structures with the fixed thermal parameters of disordered atoms and were not refined in further calculations. The hydrogen atoms at the carbon atoms and ligands μ_3-OH (compound **V**) were calculated from the geometric concepts and taken into account in the riding model. The hydrogen atoms of the coordinated water molecules (compound **V**) were calculated from the difference Fourier synthesis and fixed in subsequent calculations. The ratio of domains in the centrosymmetric twin of **V** was 0.512 : 0.488 [17]. The structures were refined by the full-matrix anisotropic–isotropic (some disordered atoms) least-squares method. All calculations were performed using the SHELXS-2013 and SHELXL-2013 programs [18].

Selected structural data are presented in Tables 1 and 2. The experimental data for compounds **I–VI** were deposited with the Cambridge Crystallographic Data Centre (CCDC 1023342 (**I** at 150 K), 1023343 (**I** at 296 K), 1023344 (**II** at 120 K), 1023345 (**II** at 180 K), 1023346 (**II** at 240 K), 1023347 (**II** at 296 K), 1023348 (**III**), 1023349 (**IV**), 1023350 (**V**), and 1023356 (**VI**), respectively; deposit@ccdc.cam.ac.uk or http://www.ccdc.cam.ac.uk/data_request/cif).

RESULTS AND DISCUSSION

Crystalline cymantrenecarboxylates $[Ln_2(\mu\text{-}O,\eta^2\text{-}O_2CCym)_2(\mu_2\text{-}O,O'\text{-}O_2CCym)_2(\eta^2\text{-}O_2CCym)_2(DMSO)_4]$ (Ln = Tb (**I**), Dy (**II**)) were obtained by the reaction of cymantrenecarboxylic acid, KOH, and $LnCl_3 \cdot 6H_2O$ in a ratio of 3 : 3 : 1 in methanol in the presence of DMSO followed by the extraction of the product with toluene. In the case of using nitrates (in the ratio 2 : 2 : 1) in a similar reaction, complexes $[Ln_2(\mu_2\text{-}O,O'\text{-}O_2CCym)_4(\eta^2\text{-}NO_3)_2(DMSO)_4]$ (Ln = Tb (**III**), Dy (**IV**)) were isolated after extraction. It should be mentioned that complexes **III** and **IV** are also formed at a reactant ratio of 3 : 3 : 1 when nitrates are used in the exchange reaction; i.e., the third NO_3 group is not substituted. Probably, it is difficult to substitute the last NO_3 group because of its bidentate character and steric hindrances of the cymantrenecarboxylate anion. The substances are light yellow crystals that are readily soluble in DMSO, THF, pyridine, CH_3CN, and CH_2Cl_2, poorly soluble in aromatic solvents, and insoluble in hexane.

Structures **I** and **II** are formed by dimers typical of lanthanide carboxylates (Fig. 1). Earlier we have synthesized and structurally characterized cymantrenecarboxylates $[Ln_2(\mu\text{-}O,\eta^2\text{-}O_2CCym)_2(\mu_2\text{-}O,O'\text{-}O_2CCym)_2(\eta^2\text{-}O_2CCym)_2(DMSO)_4]$ (Ln = Ce, Nd, Eu, and Gd) isoformular to complexes **I** and **II** [8]. The X-ray diffraction analysis for the Nd compound was carried out at 150 K, whereas for other compounds X-ray diffraction analyses were carried out at 296 K. In all cases, the space group was unambiguously determined as $P2_1/c$, $Z = 2$ (the dimer is centrosymmetric). The X-ray diffraction analysis of compound **I** at 150 K shows the space group $P2_1$ for similar unit cell parameters (the complex is in the general position), whereas at 296 K the space group is transformed into $P2_1/c$ (the experiments were carried out for the same single crystal). This means that at room temperature all compounds are isostructural, whereas for a temperature decrease to 150 K compound **I** undergoes the phase transition. Complex **II** is isostructural with compound **I** and undergoes a similar transformation.

The X-ray diffraction analyses of the same single crystal were carried out at 120, 180, 240, and 296 K to reveal specific features of the structural rearrangement of compound **II** at different temperatures. After each experiment, the crystal was stored for 1 h to attain equilibrium after the temperature increase. The increase in the unit cell volume of compound **II** is symbate to temperature: at 296 K the space group is $P2_1/c$, and at lowered temperatures it is $P2_1$ (Table 1). The structural rearrangement occurs gradually with temperature: the structures of two topologically identical but crystallographically independent halves of dimer $[Dy_2(\mu\text{-}O,\eta^2\text{-}O_2CCym)_2(\mu_2\text{-}O,O'\text{-}O_2CCym)_2(\eta^2\text{-}O_2CCym)_2(DMSO)_4]$ more and more coincide with each other, and at 296 K the intrinsic symmetry of the

Table 1. Selected structural data and refinement results for compounds **I** and **II**

Parameter	Value					
	I at 150 K	**I** at 296 K	**II** at 120 K	**II** at 180 K	**II** at 240 K	**II** at 296 K
T, K	150(2)	296(2)	120(2)	180(2)	240(2)	296(2)
Crystal system	Monoclinic	Monoclinic	Monoclinic	Monoclinic	Monoclinic	Monoclinic
Space group	$P2_1$	$P2_1/c$	$P2_1$	$P2_1$	$P2_1$	$P2_1/c$
a, Å	11.8119(2)	13.1783(7)	11.7982(4)	11.8269(3)	11.8618(2)	13.1735(2)
b, Å	24.3374(4)	24.5983(13)	24.3120(7)	24.3936(6)	24.4929(5)	24.5831(4)
c, Å	13.0393(2)	11.9169(6)	13.0240(4)	13.0688(3)	13.1166(3)	11.9080(2)
β, deg	100.7950(10)	100.167(2)	100.7460(10)	100.5880(10)	100.3630(10)	100.1850(10)
V, Å^3	3682.09(10)	3802.4(3)	3670.3(2)	3706.16(16)	3748.60(13)	3795.58(11)
Z	2	2	2	2	2	2
ρ(calcd.), g/cm^3	1.906	1.845	1.918	1.900	1.878	1.855
μ, mm^{-1}	3.090	2.993	3.209	3.178	3.142	3.103
F(000)	2072	2072	2076	2076	2076	2076
Crystal size, mm	0.3 × 0.2 × 0.16	0.3 × 0.2 × 0.16	0.35 × 0.2 × 0.18	0.35 × 0.2 × 0.18	0.35 × 0.2 × 0.18	0.35 × 0.2 × 0.18
θ Range, deg	2.294–30.594	2.281–30.557	2.298–30.570	2.293–30.548	2.289–30.539	2.282–30.543
Index range	$-16 \le h \le 16$, $-34 \le k \le 34$, $-18 \le l \le 17$	$-18 \le h \le 18$, $-35 \le k \le 35$, $-17 \le l \le 17$	$-16 \le h \le 16$, $-34 \le k \le 34$, $-18 \le l \le 18$	$-16 \le h \le 16$, $-32 \le k \le 34$, $-18 \le l \le 18$	$-16 \le h \le 16$, $-32 \le k \le 34$, $-18 \le l \le 18$	$-18 \le h \le 18$, $-34 \le k \le 35$, $-17 \le l \le 17$
All reflections	37270	124483	52192	35214	35537	55498
Independent reflections (R_{int})	21233 (0.0355)	11616 (0.0381)	21831 (0.0306)	21366 (0.0271)	21567 (0.0279)	11521 (0.0414)
Completeness to θ = 25.242°, %	99.9	99.9	99.9	99.9	99.9	99.9
Max, min transmission	0.6478, 0.4191	0.6478, 0.4239	0.6478, 0.4012	0.6478, 0.4038	0.6478, 0.4076	0.6478, 0.398
Restraints/parameters	13/990	42/543	13/990	13/999	61/979	18/497
Goodness-of-fit	0.981	1.407	1.017	0.995	0.980	1.338
R_1, wR_2 ($I > 2\sigma(I)$)	0.0375, 0.0717	0.0613, 0.1283	0.0270, 0.0599	0.0341, 0.0670	0.0389, 0.0795	0.0671, 0.1289
R_1, wR_2 (all array)	0.0451, 0.0750	0.0711, 0.1321	0.0296, 0.0610	0.0410, 0.0697	0.0504, 0.0848	0.0851, 0.1344
Flack parameter	0.487(7)		0.416(5)	0.394(7)	0.314(8)	
Max, min peaks, e/Å^3	1.418, –1.239	1.996, –1.244	1.212, –1.258	0.916, –0.810	0.957, –0.817	1.615, –1.118

Table 2. Selected structural data and refinement results for compounds **III**–**VI**

Parameter	Value			
	III	**IV**	**V**	**VI**
T, K	295(2)	295(2)	173(2)	160(2)
Crystal system	Triclinic	Triclinic	Orthorhombic	Triclinic
Space group	$P\bar{1}$	$P\bar{1}$	$Pna2_1$	$P\bar{1}$
a, Å	11.3142(5)	11.3305(10)	28.648(2)	13.7657(8)
b, Å	11.9015(6)	11.9093(10)	23.5027(17)	14.7652(9)
c, Å	13.2621(6)	13.2664(11)	19.4926(14)	17.4282(10)
α, deg	82.8110(10)	82.728(2)	90	66.7620(10)
β, deg	66.8510(10)	66.8650(10)	90	68.3490(10)
γ, deg	67.3000(10)	67.2820(10)	90	67.0200(10)
V, Å^3	1514.10(12)	1517.8(2)	13124.5(16)	2898.3(3)
Z	1	1	4	1
ρ(calcd.), g/cm^3	1.911	1.914	1.770	1.782
μ, mm^{-1}	3.339	3.462	3.097	2.526
F(000)	852	854	6900	1541
Crystal size, mm	0.3 × 0.15 × 0.15	0.2 × 0.12 × 0.1	0.2 × 0.15 × 0.12	0.32 × 0.3 × 0.25
θ Range, deg	2.309–28.364	2.306–28.378	2.302–27.528	2.322–30.032
Index range	$-15 \le h \le 13$, $-15 \le k \le 15$, $-17 \le l \le 17$	$-14 \le h \le 15$, $-15 \le k \le 15$, $-14 \le l \le 17$	$-37 \le h \le 37$, $-30 \le k \le 30$, $-25 \le l \le 25$	$-19 \le h \le 19$, $-20 \le k \le 20$, $-24 \le l \le 24$
All reflections	14844	14368	149379	34288
Independent reflections (R_{int})	7392 (0.0267)	7428 (0.0327)	30101 (0.0623)	16823 (0.0222)
Completeness to θ = 25.242°, %	99.5	99.6	99.9	99.9
Max, min transmission	0.6471, 0.3983	0.6035, 0.4675	0.7456, 0.6316	0.4935, 0.2411
Restraints/parameters	0/410	0/406	55/1353	0/805
Goodness-of-fit	1.016	0.971	1.216	1.023
R_1, wR_2 ($I > 2\sigma(I)$)	0.0281, 0.0621	0.0356, 0.0756	0.0505, 0.1359	0.0283, 0.0720
R_1, wR_2 (all array)	0.0353, 0.0652	0.0485, 0.0826	0.0780, 0.1574	0.0336, 0.0751
Max, min peaks, e/Å^3	0.625, −0.623	0.621, −1.030	2.489, −2.054	1.825, −1.159

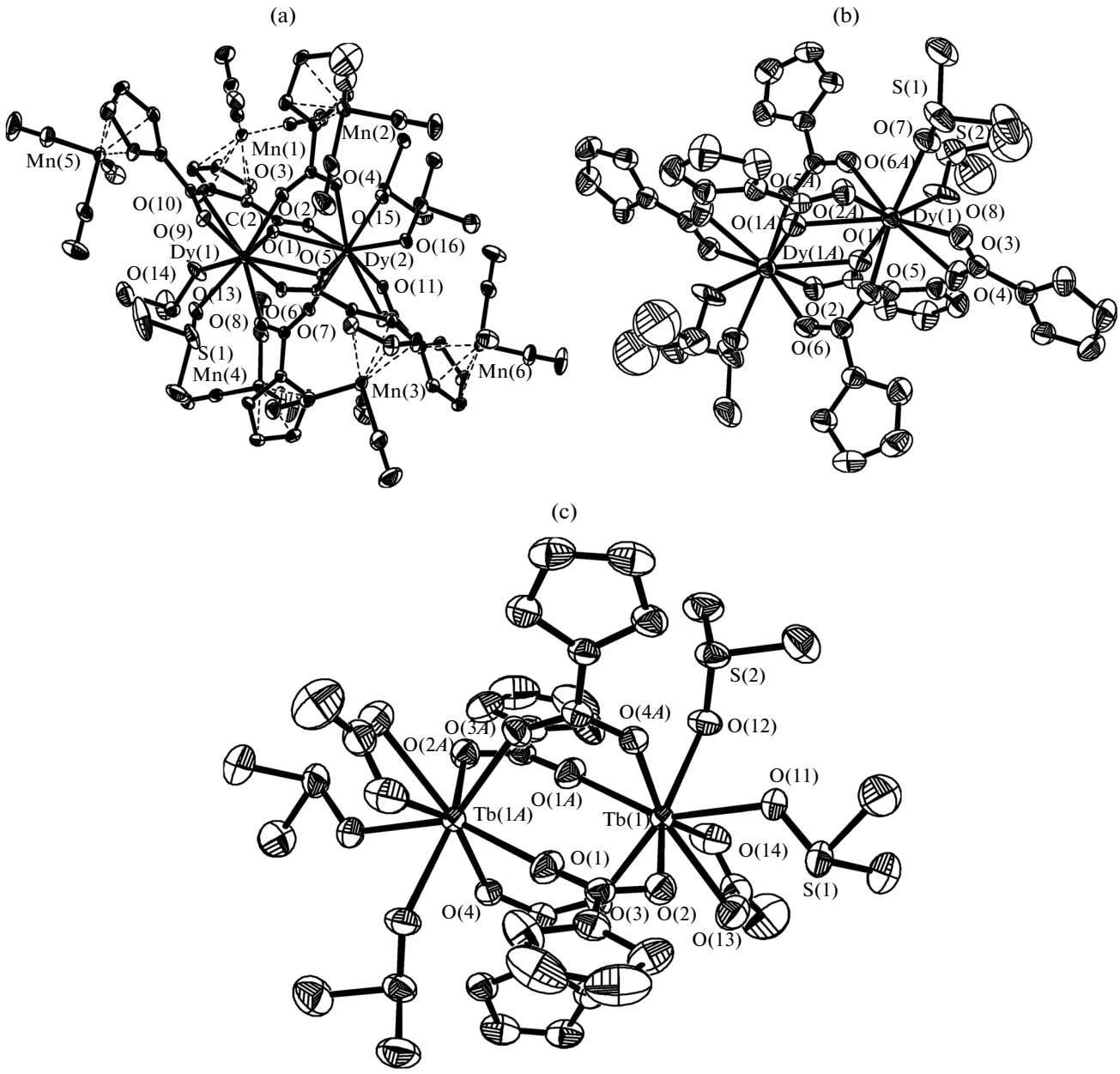

Fig. 1. Structures of complexes (a) **II** at 120 and (b) 296 K and (c) **III**. The $Mn(CO)_3$ fragments are omitted for (b) and (c).

complex (–1) is transformed into the crystallographic one (Figs. 1a and 1b).

A decrease in the medium intensity of reflections (forbidden for the *z* plane) with temperature is shown in Fig. 2. This is an ideal linear dependence. It is most likely that the transition is due to the enhancement of thermal vibrations of atoms, which is seen in Figs. 1a and 1b presenting 50% probability ellipsoids. The difference in structures of two halves of the dimer is very low (the maximum difference is observed for the turn of the DMSO molecules and $Mn(CO)_3$ fragments), and with the temperature increase the temperature vibrations reduce these differences to minimum. The disordering of DMSO and $Mn(CO)_3$ is observed at both 120 and 296 K but naturally increases with temperature. At 120 K for the sulfur atoms U_{eq} = 0.018–0.038 Å^2. Thus, some disordering is observed in spite of the fact that each of four sulfur atoms occupies one position. This is confirmed by the necessity to impose restraints on the thermal vibrations of two carbon atoms of the DMSO molecule with the maximum value of U_{eq} of the sulfur atom. Two carbonyl ligands of one $Mn(CO)_3$ fragment are also disordered at 120 K. At 296 K one of two DMSO molecules is disordered

over three positions. One and three CO ligands are disordered in two $Mn(CO)_3$ fragments of three.

The structure of $[Nd_2(\mu\text{-}O,\eta^2\text{-}O_2CCym)_2(\mu_2\text{-}O,O'\text{-}O_2CCym)_2(\eta^2\text{-}O_2CCym)_2(DMSO)_4]$ at 150 K retains the space group $P2_1/c$ [8] possibly due to the absence of a phase transition for light Ln atoms and a decrease in the transition temperature to >150 K. It is well seen for compound **II** used as an example that the Ln···Ln' distance in the tetranuclear carboxylate dimers correlates with the bond length of the lanthanide atom with the μ-O atom of the $\mu\text{-}O,\eta^2\text{-}O_2CCym$ ligand: the Ln–O bond lengths remain nearly unchanged with the temperature change (Table 3) except for the bridging Ln–O(1) bond. The change in the Ln···Ln' distance is also symbate.

Isostructural crystals of compounds **III** and **IV** are formed by centrosymmetric dimers $[Ln_2(\mu_2\text{-}O,O'\text{-}O_2CCym)_4(\eta^2\text{-}NO_3)_2(DMSO)_4]$ (Ln = Tb (**III**), Dy (**IV**)). The structures of the dimers are close to those found for compounds **I** and **II** taking into account the replacement of the $\eta^2\text{-}O_2CCym$ ligand by $\eta^2\text{-}NO_3$. On going from compounds **I** and **II** to compounds **III** and **IV**, the $\mu\text{-}O,\eta^2\text{-}O_2CCym$ ligands are slightly unfolded in such a way that they become $\mu_2\text{-}O,O'\text{-}O_2CCym$, resulting in a decrease in the coordination number of the Ln atom from 9 (**I** and **II**) to 8 (**III** and **IV**). The Ln–O(1) distances (μ-O in compounds **III** and **IV**, Fig. 1c) are 3.050 and 3.015 Å in compounds **III** and **IV**, respectively, resulting, as mentioned above, in some elongation of the Ln···Ln' distance (4.1864(3) (**III**) and 4.1775(4) Å (**IV**)). In [8] we ascribed the isolation of the forms $Ln_2(\mu\text{-}O,\eta^2\text{-}O_2CR)_2(\mu_2\text{-}O,O'\text{-}O_2CR)_2$ or $Ln_2(\mu_2\text{-}O,O'\text{-}O_2CR)_4$ in the solid phase to a compromise between the nature of Ln and packing factors of the crystal structure.

In our previous studies we showed the possibility to use the cymantrenecarboxylate fragment as a source of Mn^{2+} ions for the formation of the Mn(II)–Ln complexes [19]. As a result of the destruction of the $CymCO_2$ fragment in the presence of the corresponding Ln^{3+} ions in various media, new polynuclear complexes $[Tb_4(\mu_3\text{-}OH)_4(\mu_2\text{-}O,O'\text{-}O_2CCym)_6(H_2O)_3(THF)_4][MnCl_4] \cdot 4CH_2Cl_2 \cdot 6THF$ (**V**) and $[Er_2Mn(\mu_2\text{-}O_2CCym)_6(\eta^2\text{-}O_2CCym)_2((MeO)_3PO)_4] \cdot 2MePh$ (**VI**) were isolated in a low yield. Structure **V** is formed by cationic complexes $[Tb_4(\mu_3\text{-}OH)_4(\mu_2\text{-}O,O'\text{-}O_2CCym)_6(H_2O)_3(THF)_4]^{2+}$ (Figs. 3a and 3b), anions $[MnCl_4]^{2-}$, and solvate molecules CH_2Cl_2 and THF. The cubane-like fragment $[Ln_4(\mu_3\text{-}OH)_4]^{8+}$ (Fig. 3b) is met in 66 compounds presented in the CCDC (version 5.35, May 2014 [20]). In 18 cases of them, the Ln^{3+} ions are additionally bound by six carboxylate ligands (one ligand per each face of the cube) to form $Ln_4(\mu_3\text{-}OH)_4(\mu_2\text{-}O,O'\text{-}O_2CR)_6$. In the last fragment, the Ln atom coordinates six oxygen atoms, and additional ligands build up the Ln polyhedron to the coordination number 7–9. In our case, three terbium atoms (Tb(2)–Tb(4)) coordinate one H_2O molecule and one THF molecule each (coordination number 8), and the fourth Tb(1) atom coordinates one THF molecule

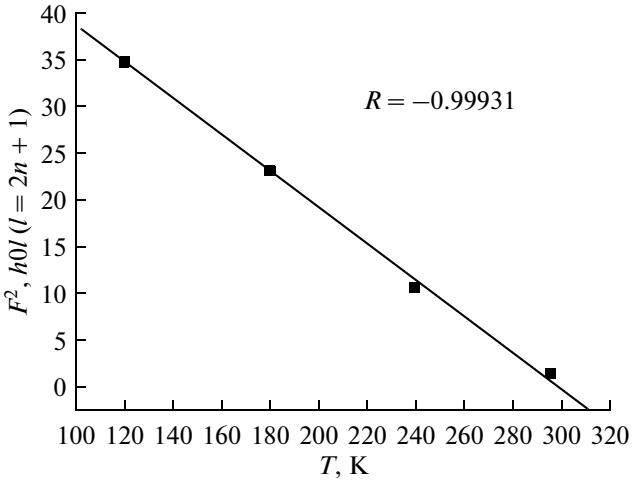

Fig. 2. Temperature dependences of the medium intensity of reflections *h*0*l* for structure **II**.

(coordination number 7). A similar combination of coordination numbers was found in five compounds [21, 22]. The Tb···Tb' distances equal to 3.80–3.82 Å (Table 2) are substantially shorter than those in compounds **I** and **II**.

If $CymCO_2^-$ is considered as carboxylate ligand L, then complex $[Er_2Mn(\mu\text{-}O,\eta^2\text{-}O_2CCym)_4(\mu_2\text{-}O_2CCym)_2(\eta^2\text{-}O_2CCym)_2((MeO)_3PO)_4]$ (Fig. 3c) in compound **VI** contains the centrosymmetric trinuclear fragment $Er(\mu_2\text{-}L)_2Mn(\mu_2\text{-}L)_2Er$. There are no similar 3d-4f-complexes in CCDC. In complex **VI**, two $\mu\text{-}O,\eta^2\text{-}O_2CCym$-ligands and one $\mu_2\text{-}O_2CCym$ ligand unify the Er and Mn atoms. The Mn atom localized in the inversion center exists in the octahedral environment. The oxygen atoms of bridging O_2CCym occupy five sites in the Er polyhedron, and the $\eta^2\text{-}O_2CCym$ ligands and two $OP(OMe)_3$ molecules build up the environment of Er to the coordination number 9. The fragments $Ln(\mu_2\text{-}L)_2M(\mu_2\text{-}L)_2Ln$ (M is 3*d* metal) can conventionally be distinguished in the polymer compounds $[ZnEu_2(Fur)_8 \cdot 2H_2O]_n$ (HFur is α-furancarboxylic acid) [23] and $[Ln_2M(O_2CMe)_8]_n \cdot 2n(HO_2CMe)$ [24] and in the pentanuclear complex $[Gd_2Mn_3(O_2C\{Me\}{=}CH_2)_{12}Bipy_2]$ [25]. It should be mentioned that, unlike Ln_2M, trinuclear complexes with the stoichiometry LnM_2 are widely abundant.

The solid-phase thermolysis of all the four complexes **I**–**IV** is staged. The first stage in an inert atmosphere corresponds to the removal of the neutral ligand (DMSO). The characteristics of thermolysis for of complexes **I**–**IV** are given in Table 4. The dependences of the changes in the mass and the heat flow on heating of complex **II** are presented in Fig. 4a. A similar character of the DSC curve was observed [26] for the thermolysis of complexes $LnCl_3 \cdot 3DMSO$.

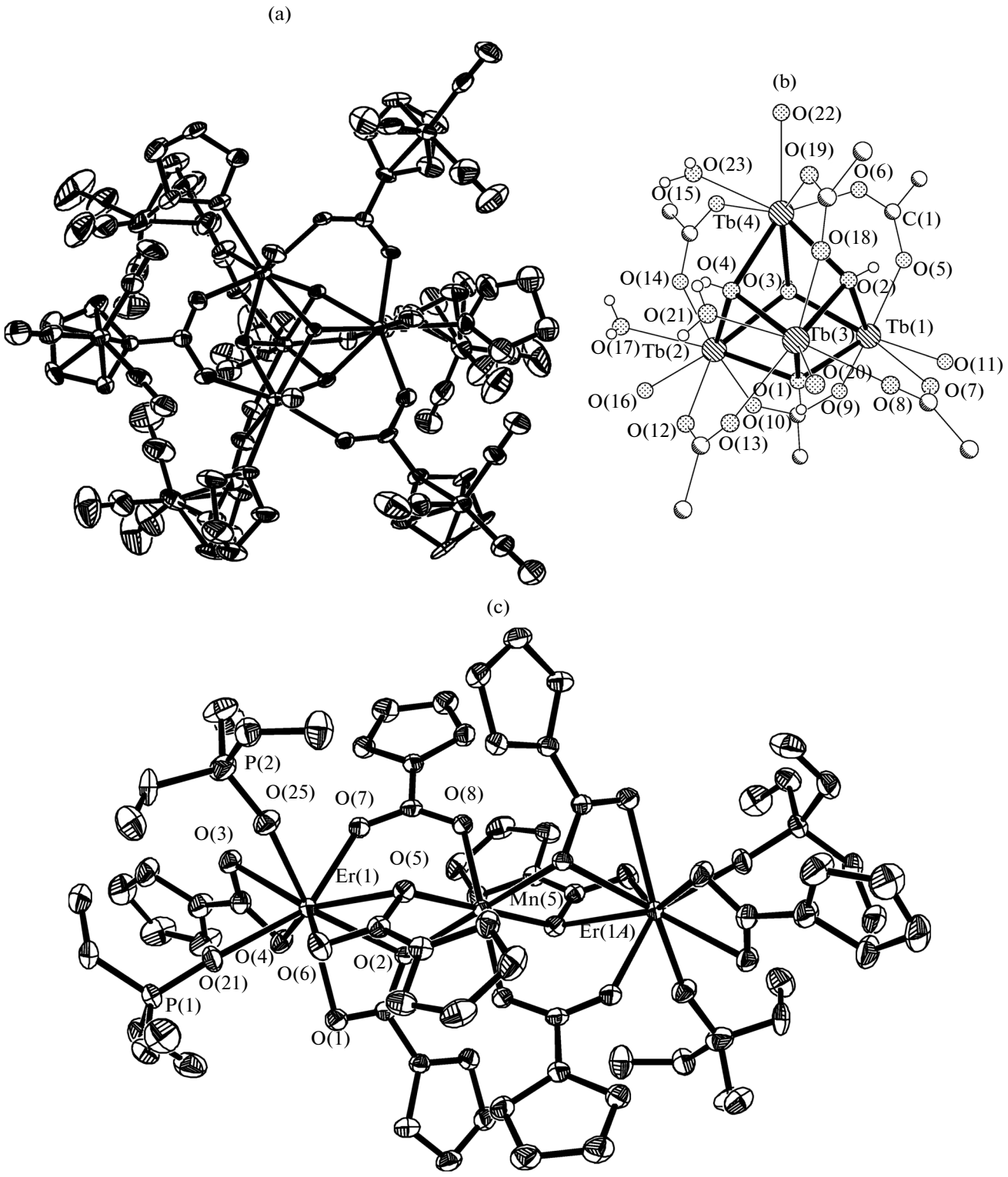

Fig. 3. (a) Structure of complex **V**, (b) the tetranuclear cationic fragment in structure **V** (the O_2CCym fragment is drawn as O_2CC, the H_2O and OH ligands are shown with the hydrogen atoms, and the coordinated THF molecules are drawn as oxygen atoms), and (c) structure **VI**.

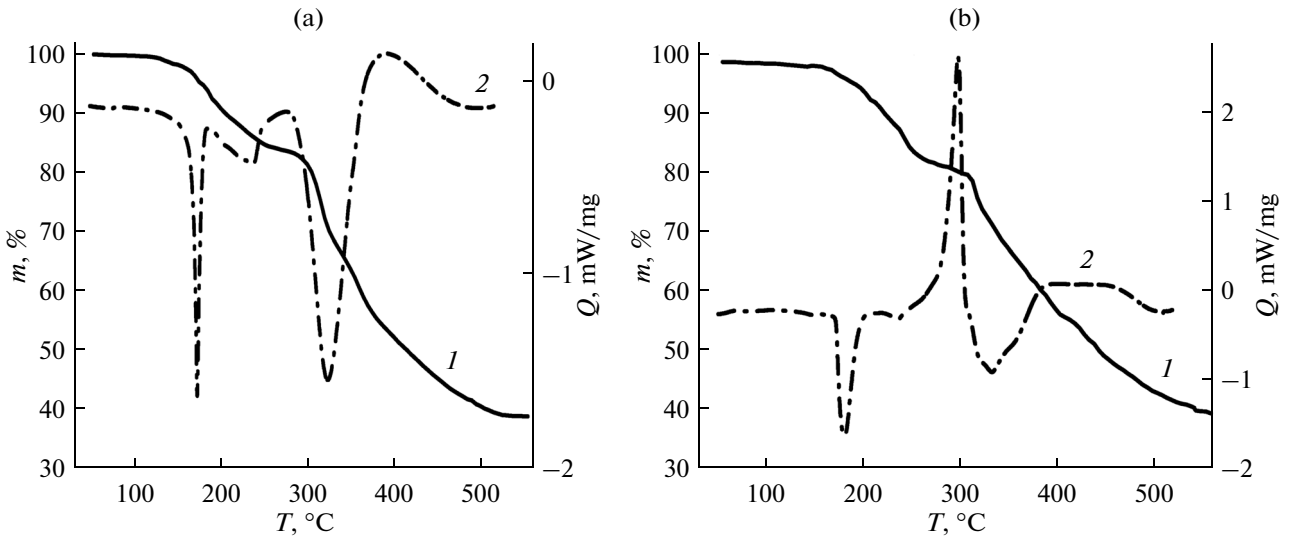

Fig. 4. Temperature dependences of the (*1*) mass change and (*2*) heat flow in an argon atmosphere for complexes (a) **II** and (b) **IV**.

According to the experimental data (Table 3), complexes **I–IV** start to decompose at temperatures higher than 150°C, which is lower than the boiling point of DMSO (189°C). Probably, at the first stage, the Ln–$OS(CH_3)_2$ bond is cleaved and the ligand begins to decompose. We have earlier showed that during the thermolysis of the DMSO-containing complexes the disproportionation of DMSO to $(CH_3)S$ and $(CH_3)_2SO_2$ takes place [8], which is confirmed by the mass spectrum of the gas phase of complex **II** under the thermogravimetric experimental conditions (the presence of ionic current peaks with m/z = 94 $[(CH_3)_2SO_2]^+$, 78 $[(CH_3)_2SO]^+$, and 47 $[(CH_3)S]^+$) (Fig. 5a). The decarbonylation of the $[(O_2CCp)Mn(CO)_3]^-$ fragment occurs at the second stage for complexes **I** and **II**, and the ions C^+(12) and CO^+(28) are detected in the mass spectrum. The mass loss at this stage corresponds to the content of carbonyl groups calculated from the empirical formula (within the experimental error) (Table 4). The further mass decrease and the formation of the final solid decomposition products are observed above 335 ± 2°C for complexes **I** and **II**. The main distinction of the solid-phase thermolysis of complexes **III** and **IV** from the thermolysis of compounds **I** and **II** is due to the presence of chelate ligands of different nature in these complexes: the $CymCO_2$ anions (in the case of complexes **I** and **II**) and the NO_3 anions (in the case of compounds **III** and **IV**). On heating complexes **III** and **IV** above 270°C, the DSC curve exhibits a significant exotherm transforming into an endotherm with further heating (Fig. 4b), and the ionic current peaks with m/z = 30 $[NO]^+$, 28 $[CO]^+$, and 44 $[CO_2]^+$ are detected in the mass spectrum. In this case, the partial oxidative destruction of the cymantrenecarboxylate fragments (due to chelate NO_3^-) and their complete decarbonylation occur. This is indicated by the intense peak with m/z = 30 in the mass spectrum corresponding to the molecular ion NO^+, which is the product of ionization of NO formed due to the reduction of the NO_3 group (Fig. 5c). The mass loss in the range of 240–400°C (Table 4) corresponds to the calculated content of the CO and NO_3 groups (within the experimental error). Above 400°C the mass loss is strongly retarded and completed at a sufficiently high temperature (800–850°C). We failed to obtain crystalline solid thermolysis products of complexes **III** and **IV** in an inert atmosphere. For the solid-phase thermolysis of complexes **III** and **IV**, the coordinated ligand is also removed in an air flow at the first stage and the organic moiety of the molecule is removed in one stage with the further heating in the range 250–460°C. The process is accompanied by a strong exotherm and affords $LnMn_2O_5$.

The magnetic properties of the lanthanide complexes are interesting and promising due to the high magnetic moment and high magnetic anisotropy of certain Ln^{3+} ions, which allows these complexes to serve, in particular, as single-molecule magnets. The 3*d*–4*f* heterometallic complexes are especially interesting in respect of the magnetic properties [27, 28]. However, exchange interactions are also possible in the homometallic binuclear lanthanide complexes [29]. The temperature dependences of the magnetic susceptibility for complexes **I**, **II**, **V**, and **VI** were studied in the range 300–2 K.

For complex **I**, at 300 K $\chi_M T = 23.813$ cm^3 mol^{-1} K, which is close to the calculated value (23.64 cm^3 mol^{-1} K

Table 3. Bond lengths Ln–O and distances Ln···Ln (Å) in structures **I** and **II**

Bond	**I** at 150 K	**II** at 120 K	**II** at 180 K	**II** at 240 K	Bond	**I**_296 K	**II**_296 K
	d, Å					*d*, Å	
Ln(1)–O(1)	2.321(4)	2.306(3)	2.311(3)	2.316(4)	Ln(1)–O(1)	2.334(4)	2.316(4)
Ln(1)–O(3)	2.361(5)	2.348(3)	2.352(4)	2.353(5)	Ln(1)–O(1*A*)	2.726(4)	2.735(5)
Ln(1)–O(5)	2.703(4)	2.699(3)	2.706(4)	2.721(5)	Ln(1)–O(2*A*)	2.416(4)	2.404(5)
Ln(1)–O(6)	2.413(5)	2.391(3)	2.396(4)	2.402(6)	Ln(1)–O(3)	2.507(5)	2.498(5)
Ln(1)–O(8)	2.368(5)	2.352(3)	2.346(4)	2.351(5)	Ln(1)–O(4)	2.467(5)	2.455(5)
Ln(1)–O(9)	2.546(4)	2.531(3)	2.519(4)	2.511(5)	Ln(1)–O(5)	2.364(4)	2.351(5)
Ln(1)–O(10)	2.423(5)	2.410(3)	2.425(4)	2.438(5)	Ln(1)–O(6*A*)	2.372(4)	2.358(5)
Ln(1)–O(13)	2.412(4)	2.406(3)	2.414(4)	2.417(5)	Ln(1)–O(7)	2.440(4)	2.428(5)
Ln(1)–O(14)	2.398(5)	2.382(4)	2.370(5)	2.367(6)	Ln(1)–O(8)	2.374(5)	2.375(11)
Ln(2)–O(1)	2.650(4)	2.637(3)	2.665(4)	2.693(5)	Ln(1)–O(82)		2.34(3)
Ln(2)–O(2)	2.439(5)	2.425(3)	2.413(4)	2.403(5)	Ln(1)···Ln(1*A*)	4.0541(6)	4.0513(6)
Ln(2)–O(4)	2.412(4)	2.400(3)	2.386(4)	2.363(5)			
Ln(2)–O(5)	2.334(4)	2.322(3)	2.321(4)	2.318(4)			
Ln(2)–O(7)	2.355(4)	2.350(3)	2.352(4)	2.353(5)			
Ln(2)–O(11)	2.452(4)	2.439(3)	2.449(4)	2.467(4)			
Ln(2)–O(12)	2.491(4)	2.493(3)	2.488(4)	2.477(5)			
Ln(2)–O(15)	2.428(4)	2.416(3)	2.423(4)	2.439(5)			
Ln(2)–O(16)	2.379(4)	2.363(3)	2.360(5)	2.369(6)			
Ln(1)···Ln(2)	4.0131(4)	4.0058(3)	4.0220(3)	4.0367(4)			

Table 4. Characteristics of the thermolysis of complexes **I**–**IV**

Characteristic	**I**	**II**	**III**	**IV**
In argon flow				
T_{in} (±2.0), °C	155	156.7	160.5	160.0
$T_{in\ 1\ st}$ (±2.0), °C	240.9	255.0	260.0	263.5
$Q_{1\ st}$ (±8.0), kJ/mol	352.0	355.5	370.2	372.0
Content of $DMSO_{calcd}$, wt %	14.76	14.72	17.90	17.83
$\Delta m_{1\ st}$ (±1.0), %	15.8	15.5	17.8	16.7
$T_{in\ 2\ st}$ (±2.0), °C	282.0	283.8	270.5	271.7
$T_{fin\ 2\ st}$ (±2.5), °C	335.5	332.5	400.0	397.6
Content of CO_{calcd}, wt %	23.85	23.77		
Content of $(CO + NO_3^-)_{calcd}$, wt %			26.39	26.28
$\Delta m_{2\ st}$ (±2.0), %	20.7	21.5	25.4	27.3
Product (X-ray diffraction analysis)	Tb_2O_3 and MnO	Amorphous	Amorphous	Amorphous
In air flow				
T_{in} (±2.0), °C	152	150	160	158
Product (X-ray diffraction analysis)	$TbMn_2O_5$ and Mn_2O_3	$DyMn_2O_5$ and Mn_2O_3	$TbMn_2O_5$	$DyMn_2O_5$

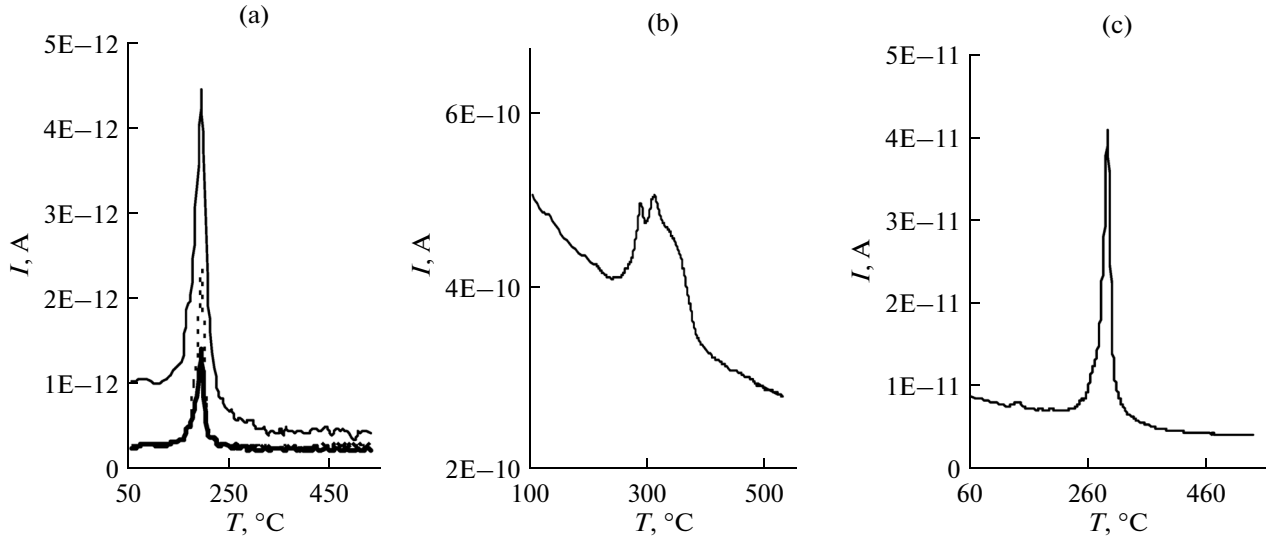

Fig. 5. Mass spectrum of the gas phase in argon under the thermogravimetric experimental conditions; ionic current peaks (m/z): (a) 94 $[(CH_3)_2SO_2]^+$ (---), 78 $[(CH_3)_2SO]^+$ (—), and 47 $[(CH_3)S]^+$ (—); (b) 44 $[CO_2]^+$ for complex **II**; and (c) 30 $[NO]^+$ for complex **III**.

[27]). With the temperature decrease this value decreases, and an especially sharp decrease is observed below 30 K (Fig. 6a). The temperature dependence of the inverse magnetic susceptibility $1/\chi$ for complex **I** in the range 33–300 K is well described by the Curie–Weiss law ($\chi(T) = C/(T-\theta)$) with constants $C = 23.863 \pm 0.036$ cm^3 mol^{-1} K and $\theta = -1.849 \pm 0.243$ K.

For complex **II**, at 300 K $\chi_M T = 28.715$ cm^3 mol^{-1} K, which is also close to the calculated value (28.34 cm^3 mol^{-1} K [27]). The temperature change in this value is similar to the previous case (Fig. 6a). The temperature dependence of the inverse magnetic susceptibility $1/\chi$ in the range 33–300 K corresponds to the Curie–Weiss law with constants $C = 28.934 \pm 0.050$ cm^3 mol^{-1} K and $\theta = -3.616 \pm 0.280$ K.

For complex **V**, at 300 K $\chi_M T = 52.197$ cm^3 mol^{-1} K, which is also close to the calculated value for four Tb^{3+} ions and Mn^{2+} ion (51.625 cm^3 mol^{-1} K). This value decreases with a decrease in the temperature (Fig. 6b). The magnetic behavior of complex **V** in the range 33–300 K is well described by the Curie–Weiss law with constants $C = 53.147 \pm 0.265$ cm^3 mol^{-1} K and $\theta = -9.239 \pm 0.836$ K. The substantial negative value of the Weiss constant indicates pronounced antiferromagnetic interactions in the metal core of compound **V**.

For complex **VI**, at 300 K $\chi_M T = 27.169$ cm^3 mol^{-1} K, which is close to the calculated value for two Er^{3+} ions and Mn^{2+} ion (27.305 cm^3 mol^{-1} K). The value of $\chi_M T$ decreases as the temperature decreases (Fig. 6b). The magnetism of complex **VI** in the range from 40 to 300 K is described by the Curie–Weiss law with constants $C = 28.204 \pm 0.052$ cm^3 mol^{-1} K and $\theta = -12.924 \pm 0.322$ K. Like in the previous case, the significant negative value of θ can indicate antiferromagnetic interactions between the ions in structure **VI**.

Lanthanide ions are promising spin carriers for the construction of single-molecule magnets. It is expedient to use heavy lanthanide ions, Tb^{3+} (f^8, ground state $^7F_6$), Dy^{3+} (f^9, ground state $^6H_{15/2}$), and Ho^{3+} (f^{10}, ground state $^5I_8$), for the directed design of single-molecule magnets due to their uniaxial anisotropy and high spin of the ground state. Many single-molecule magnets based on the Mn complexes are also known [30].

To determine the ability of compounds to exhibit the properties of single-molecule magnets, it is necessary to measure the dynamic magnetic susceptibility in a weak alternating field, i.e., to use the method of dynamic (ac) magnetic susceptibility. In this case, the imaginary component χ'' of the ac susceptibility rather than the ac susceptibility itself ($\chi_{ac} = \chi' + \chi''$) is interesting. Such measurements have not been performed in Russia up to the present time.

We measured the ac magnetic susceptibility in the direct magnetic field with the intensity $H = 0$ and 5 kOe to confirm the assumption that the properties of complexes **II** and **VI** are characteristic of single-molecule magnets. In the zero external field, the temperature dependences of the imaginary component contain the frequency-dependent signal and a noticeable increase in χ'', but no distinctly detected maximum was observed. The application of an external magnetic field results in a decrease in the probability of quantum tunneling, an increase in the relaxation time, and, as a result, the possibility to observe the properties of single-molecule magnets at higher temperature [31]. As the field intensity increases to $H = 5$ kOe, the maxi-

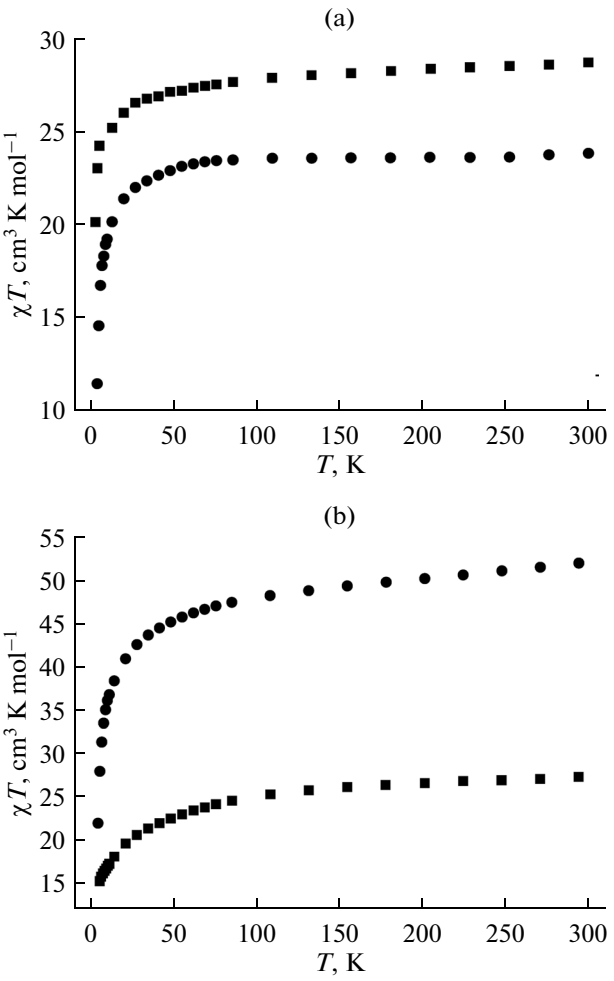

Fig. 6. Temperature dependences $\chi_m T$ for complexes (a) **I** (●) and **II** (■), (b) **V** (●) and **VI** (■).

mum in the $\chi''(T)$ dependences is observed in the range 4.5–5 K at all frequencies at which the measurements were carried out (Fig. 7). This run of the $\chi''(T)$ dependence indicates the presence of the slow magnetic relaxation and energy barrier ΔE that should be surmounted for the reorientation of the magnetic moment of the molecule. The maximum observed in the dependence $\chi''(T)$ of complex **II** makes it possible to surely assign this complex to single-molecule magnets [32]. In the case of complex **VI**, similar measurements revealed no increase in χ'' down to 2 K; i.e., this complex does not manifest the properties of a single-molecule magnets in the accessible temperature range.

Thus, we obtained new heterometallic 3*d*–4*f* carboxylate complexes in which the transition metal is bound to the aromatic π system: $[Ln_2(\mu\text{-}O,\eta^2\text{-}O_2CCym)_2(\mu_2\text{-}O,O'\text{-}O_2CCym)_2(\eta^2\text{-}O_2CCym)_2(DMSO)_4]$ (Ln = Tb (**I**), Dy (**II**)) and $[Ln_2(\mu_2\text{-}O,O'\text{-}O_2CCym)_4(\eta^2\text{-}NO_3)_2(DMSO)_4]$ (Ln = Tb (**III**), Dy (**IV**)). The binuclear structure of complexes **I**–**IV** is typical of the lanthanide carboxylates. Complexes **I** and **II** in the range of 150–296 K exhibit an extended phase transition that appears as a change in the symmetry space group. Carboxylate clusters $[Tb_4(\mu_3\text{-}OH)_4(\mu_2\text{-}O,O'\text{-}O_2CCym)_6(H_2O)_3(THF)_4][MnCl_4] \cdot 4CH_2Cl_2 \cdot 6THF$ (**V**) and $[Er_2Mn(\mu_2\text{-}O_2CCym)_6(\eta^2\text{-}O_2CCym)_2((MeO)_3PO)_4] \cdot 2MePh$ (**VI**) containing Mn^{2+} ions formed due to the partial destruction of the $CymCO_2$ fragment in solution were also synthesized. The structure of the core of compound **VI** is unique. The thermolysis of complexes **I**–**IV** was studied in an atmosphere of Ar and air. It is shown that this process is staged in all cases and leads, in the case of complexes **III** and **IV** in air, to $LnMn_2O_5$ phases. The magnetic behavior of complexes **I**, **II**, **V**, and **VI** in the range of 2–300 K corresponds to the predomination of antiferromagnetic interactions in all cases. The measurements in the alternating magnetic field show that complex **II** is a single-molecule magnet.

ACKNOWLEDGMENTS

This work was supported by the Russian Scientific Foundation, project no. 14-13-00938.

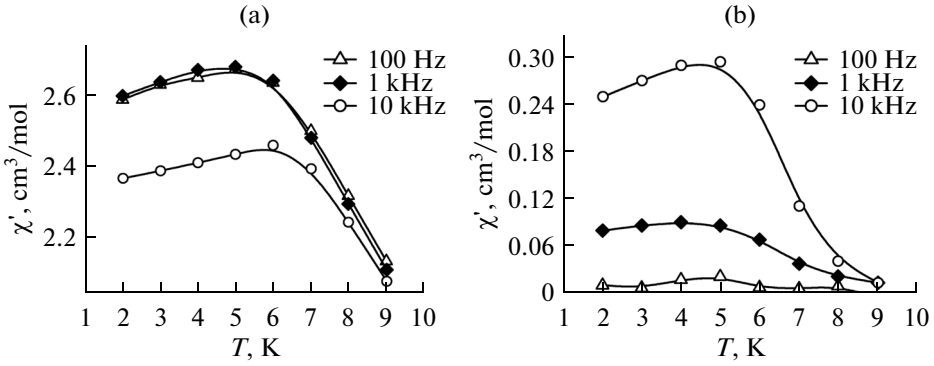

Fig. 7. Temperature dependences of the (a) real and (b) imaginary parts of the ac magnetic susceptibility of complex **II** in the external magnetic field (H = 5 kOe).

REFERENCES

1. Sakamoto Masatomi, Manseki Kazuhiro, and Okawa Hisashi, *Coord. Chem. Rev.*, 2001, vol. 219–221, p. 379.
2. Andruh, M., Costes, J.-P., Diaz, C., and Gao, S., *Inorg. Chem.*, 2009, vol. 48, p. 3342.
3. Huang You-Gui, Jiang Fei-Long, and Hong Mao-Chun, *Coord. Chem. Rev.*, 2009, vol. 253, p. 2814.
4. Sharples, J.W. and Collison, D., *Coord. Chem. Rev.*, 2014, vol. 260, p. 1.
5. Koroteev, P.S., Dobrokhotova, Zh.V., Efimov, N.N., et al., *Russ. J. Coord. Chem.*, 2014, vol. 40, no. 7, p. 495.
6. Koroteev, P.S., Kiskin, M.A., Dobrokhotova, Zh.V., et al., *Polyhedron*, 2011, vol. 30, p. 2523.
7. Koroteev, P.S., Dobrokhotova, Zh.V., Kiskin, M.A., et al., *Polyhedron*, 2012, vol. 43, p. 36.
8. Koroteev, P.S., Dobrokhotova, Zh.V., Ilyukhin, A.B., et al., *Izv. Akad. Nauk, Ser. Khim.*, 2012, no. 6, p. 1064 (Russ. Chem. Bull., Int. Ed., 2012, no. 6, p. 1069).
9. Koroteev, P.S., Dobrokhotova, Zh.V., Ilyukhin, A.B., et al., *Polyhedron*, 2013, vol. 65, p. 110.
10. Koroteev, P.S., Dobrokhotova, Zh.V., Ilyukhin, A.B., et al., *Polyhedron*, 2015, vol. 85, p. 941.
11. Pasynskii, A.A., Shapovalov, S.S., Gordienko, A.V., et al., *Inorg. Chim. Acta*, 2012, vol. 384, p. 18.
12. Pasynskii, A.A., Shapovalov, S.S., Gordienko, A.V., and Skabitskii, I.V., *Russ. J. Coord. Chem.*, 2011, vol. 37, no. 2, p. 127.
13. Shapovalov, S.S., Pasynskii, A.A., Skabitskii, I.V., et al., *Russ. J. Coord. Chem.*, 2014, vol. 40, no. 2, p. 77.
14. Maksakov, V.A., Podberezskaya, N.V., Zavodnik, V.E., et al., *Koord. Khim.*, 1986, vol. 12, no. 8, p. 1132.
15. Nesmeyanov, A.N., Anisimov, K.N., Kolobova, N.E., and Makarov, Yu.V., *Izv. Akad. Nauk SSSR, Ser. Khim.*, 1968, no. 3, p. 686.
16. *APEX2 and SAINT*, Madison (WI, USA): Bruker AXS Inc., 2007.
17. Sheldrick, G.M., *SADABS*, Göttingen (Germany): Univ. of Göttingen, 1997.
18. Sheldrick, G.M., *Acta Crystallogr., Sect. A: Found. Crystallogr.*, 2008, vol. 64, no. 1, p. 112.
19. Koroteev, P.S., Efimov, N.N., Ilyukhin, A.B., et al., *Inorg. Chim. Acta*, 2014, vol. 418, p. 157.
20. Allen, F.H., *Acta Crystallogr., Sect. B: Struct. Sci.*, 2002, vol. 58, no. 3, p. 380.
21. Ma, B.-Q., Zhang, D.-S., Gao, S., et al., *Angew. Chem., Int. Ed. Engl.*, 2000, vol. 39, no. 20, p. 3644.
22. Wang, R., Selby, H.D., Liu, H., et al., *Inorg. Chem.*, 2002, vol. 41, no. 2, p. 278.
23. Yin, M., Lei, X., Li, M., et al., *J. Phys. Chem. Solids*, 2006, vol. 67, no. 7, p. 1372.
24. Bierke, T., *Thesis Department für Chemie*, Köln (Deutschland): Univ. zu Köln, 2012.
25. Wu, B., *Dalton Trans.*, 2006, no. 43, p. 5113.
26. Matos, J.R., De Faria, Z.F., Giolito, I., et al., *Thermochim. Acta*, 1992, vol. 205, p. 253.
27. Benelli, C. and Gatteschi, D., *Chem. Rev.*, 2002, vol. 102, p. 2369.
28. Wang Bing Wu, Jiang Shang Da, Wang Xiu Teng, Gao Song, *Sci. China B*, 2009, vol. 52, p. 1739.
29. Koroteev, P.S., Efimov, N.N., Dobrokhotova, Zh.V., et al., *Izv. Ross. Akad. Nauk, Ser. Khim.*, 2013, no. 8, p. 1768 (Russ. Chem. Bull., Int. Ed., 2013, no. 8, p. 1768).
30. Aromí, G. and Brechin, E.K., *Struct. Bond*, 2006, vol. 122, p. 1.
31. Langley, S.K., Chilton, N.F., Ungur, L., et al., *Inorg. Chem.*, 2012, vol. 51, p. 11873.
32. Woodruff, D.N., Winpenny, R.E.P., and Layfield, R.A., *Chem. Rev.*, 2013, vol. 113, p. 511.

Translated by E. Yablonskaya